Additive Manufacturing Letters 6 (2023) 100153

Contents lists available at ScienceDirect

Additive Manufacturing Letters

journal homepage: www.elsevier.com/locate/addlet

Short Communication

Towards in-situ fumes composition monitoring during an additive manufacturing process using energy dispersive X-ray fluorescence spectrometry

Adrien Stolidi [a,*], Anthony Touron [a], Loïc Toulemonde [a], Hugues Paradis [a,1], Pierre Lapouge [b], Frédéric Coste [b], Jean-Paul Garandet [c]

[a] Université Paris Saclay, CEA, List, Palaiseau F91120, France
[b] Laboratoire PIMM, Arts Et Métiers Institute of Technology, CNRS, Cnam, HESAM University, Paris 75013, France
[c] Université Grenoble Alpes, CEA, Liten, Grenoble F-38000, France

ARTICLE INFO

Keywords:
In-line monitoring
LPBS
ED-XRF

ABSTRACT

We present an in-situ energy dispersive X-ray fluorescence measurement of the content of Chromium and Nickel in the fumes produced by selective laser melting on an Inconel 625 powder. Significant variations of the intensities of the Chromium and Nickel Kα fluorescence lines were evidenced as a function of the laser power, lasing velocity and chamber atmosphere. Calibration has been carried out using Monte–Carlo particle transport simulations allowed to obtain a quantitative estimate of the Chromium and Nickel mass fraction in the fumes. The experimental data has been compared to the predictions of an analytical physico-chemical model with consistent results. This approach thus also allows to provide information on the temperature of the metallic bath.

1. Introduction

In a number of Additive Manufacturing (AM) techniques (e.g. Laser Powder Bed Fusion, LPBF or Wire Arc Additive Manufacturing, WAAM), part fabrication proceeds from repeated fusion and solidification steps. The monitoring and characterization of the molten pools are therefore of paramount importance for the control of the process, and this is specially true in the Powder Bed techniques where the energy density inputs are very high. As a matter of fact, in addition to the heat transfer phenomena that define the geometry of the liquid pool, a number of processes, such as fume evaporation, spatter generation or powder denudation, take place within or in the vicinity of the melt [1]. To gain some insight into these complex phenomena, both visible and infrared cameras can be implemented within LPBF chambers [2,3]. In 2.5D samples, very accurate information on powder melting and spatter behavior can be retrieved from in situ X-ray imaging [4].

Conversely, much less attention has been paid to the chemical phenomena occurring within or in the vicinity of the melt pool, with the noticeable exception of the work carried out by Lednev et al. [5] using Laser Induced Breakdown Spectroscopy (LIBS). In Tungsten carbide (WC) reinforced Nickel-based clads, these authors were able to in situ measure both the W and C melt concentrations. More generally, such concentration measurements would be very valuable in LPBF process conditions. Indeed, in view of the high energy densities involved, a major issue regarding the chemistry of the melt pool is that a number of elements will have strong vapor pressures, especially in the vicinity of the heat source, as a consequence of the very high temperatures reached. In an alloy where constituents have significantly different evaporation temperatures (e.g. Zinc and Magnesium in Aluminium based systems), this could result in noticeable differences between the compositions of the starting and solidified materials.

Therefore the issue of monitoring the fume composition should be of interest for the AM community, and the objective of the present letter is to show that the evaporation fumes typical of a standard LPBF process on an Inconel 625 alloy can be monitored using Energy Dispersive X-ray Fluorescence (ED-XRF), an elemental analysis technique. To do so an experimental campaign has been conducted on an LPBF laboratory bench. With the help of a calibration method, these *in-process* ED-XRF measurements are able to detect mass fraction around 10^{-4} for Chromium and Nickel in the fumes. These results have been interpreted in the frame of an analytic physico-chemical model to support the overall consistency of our quantitative in-situ fumes monitoring method. An independent analysis of the Chromium and Nickel data results in fairly close agreement in terms of melt bath temperatures.

* Corresponding author.
E-mail address: adrien.stolidi@cea.fr (A. Stolidi).
[1] Current affiliation: CEA-DAM Ile-de-France, Bruyéres-le-Châtel 91297, Arpajon Cedex.

https://doi.org/10.1016/j.addlet.2023.100153
Received 31 March 2023; Received in revised form 5 May 2023; Accepted 21 May 2023

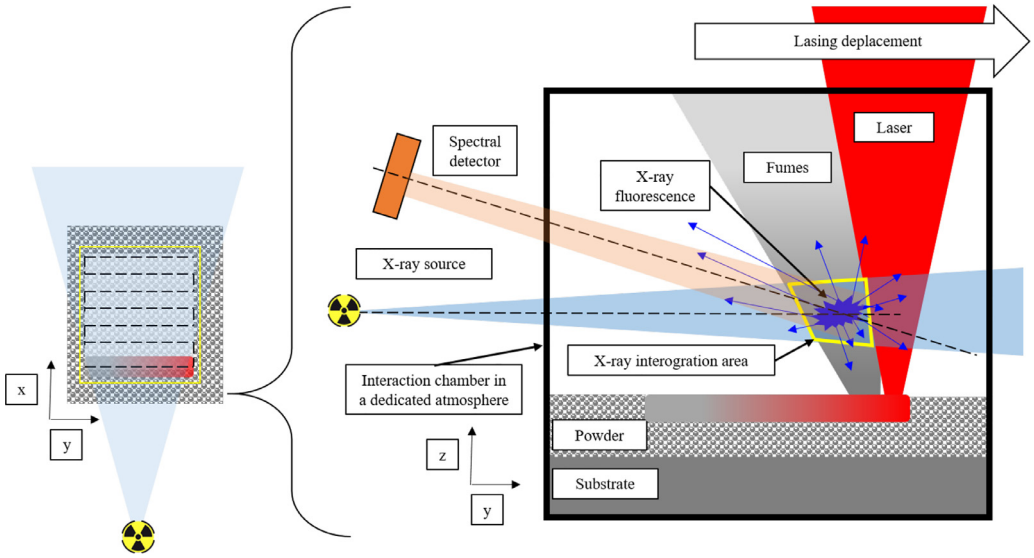

Fig. 1. Sketch of the LPBF process with fumes ED-XRF monitoring.

2. Materials and methods

2.1. *ED-XRF* in-situ *measurement of a LPBF process*

The principle of the X-ray fluorescence technique is to illuminate a material with an ionising source, for instance an X-ray tube, to induce X-ray fluorescence events. Then a detection system, for example a solid-state detector, is used to collect the fluorescence lines that will be sorted according to the photons energies (ED-XRF). The energies associated to these lines are characteristic of the elements constituting the material, allowing their identification, and with an adequate calibration it becomes possible to quantify them. Typically, the elements of the Mendeleev table ranging from Magnesium to Uranium are suitable for ED-XRF analysis.

The technique is mostly used for post-process analysis (recent work can be found in the review of Vanhoof et al. [6]), but it appeared interesting to test its potential for the in-situ monitoring of an LPBF process, the basic idea being to target the fumes in an interrogation volume above the lasing area. A schematic view of the system used is shown in Fig. 1. The interrogation volume corresponds to the intersection of the X-ray emission cone and the detector cone (shown in blue and orange in Fig. 1). These cones are based respectively on the 3 mm diameter cylindrical Lead collimator of the X-ray tube and on the 7 mm diameter cylindrical stainless steel collimator of the detector. Once the laser is set in motion along a predefined scan trajectory, its interaction with the underlying material will induce fumes above the metallic pool. The process is implemented in a specific protective atmosphere. During our experiments, a portion of the fumes is illuminated with an X-ray source resulting in X-ray fluorescence events, characteristic of the elements composing the fumes. Then, these fluorescence events are collected by a spectral detector. The fluorescence measurements are cumulative during the lasing scan.

The main parameter that contributes to element evaporation is the local melt pool temperature, which depends on a number of process parameters but also on the thermophysical properties of the alloy. In this letter, we investigated the effect of the laser nominal power and velocity, as well as the effect of the structure (powder or solid plate) of the alloy and the chemistry (Nitrogen and Helium) of the protection atmosphere.

2.2. *LPBF laboratory bench and ED-XRF material*

The setup is shown in Fig. 2. A homemade interaction chamber (label A) was designed for samples layout and isolation from the surrounding atmosphere. The laser beam (label B) passes through a transparent window at the top of the chamber (label A1) and the ED-XRF measurement system is positioned sideways with the X-ray tube and the detector represented respectively with labels C and D. As in standard LPBF machines, a cross jet is positioned above the illumined sample to evacuate the fumes. On the ED-XRF measurement side, the box is closed by a Kapton window (label A2) in order to minimize the X-ray attenuation while maintaining the chamber confinement.

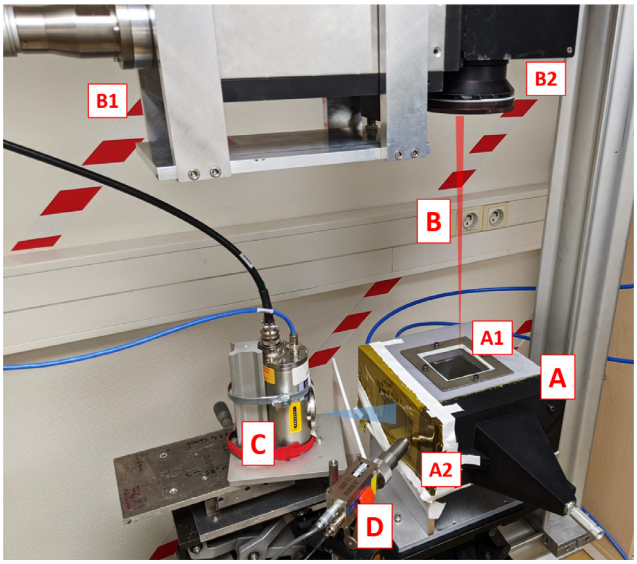

Fig. 2. Photography of the setup with the interaction chamber (A); the laser (B1) and the scanning head (B2); the X-ray tube (C) and the spectral detector (D).

A single mode 500 W laser from SPI Lasers (now Trumpf, see label B1), with a spot diameter estimated at $1/e^2 = 75$ µm and a laser trajectory control system Hurryscan 14 with a scanning head (label B2) from Scanlab and a focal lens Ftheta of 420 mm from Linos were used. As for the X-ray tube, we used the Jupiter 5000 model from Oxford Instruments (label C), with a Silver reflection target completed by an Aluminum filter of 400 µm thickness. The purpose of the filtration is to decrease the unwanted scattering contribution in the energy range of 3 to 8 keV (see green bar on energy axis in Fig. 3) as this energy range will be shown to be particularly interesting for the fumes analysis. The

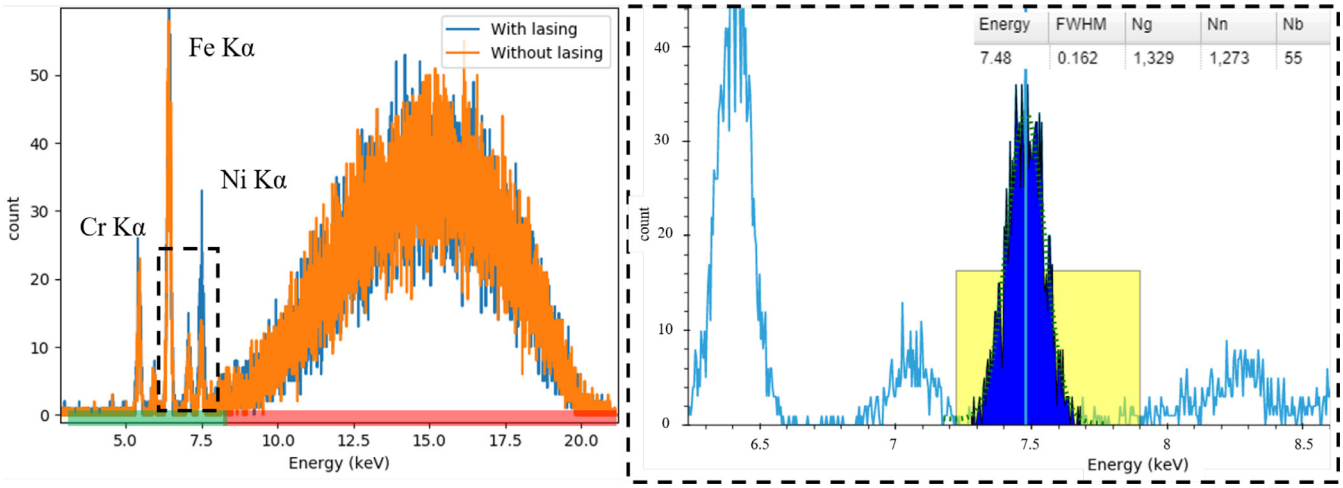

Fig. 3. Example of spectra acquisitions (left) and net counting estimation (right) for the case of Ni Kα.

maximum voltage and current were respectively of 21 kV and 1 mA. The spectral detector used was an Amptek XR-100SDD of 25 mm^2 area (label D) plugged with a multichannel analyzer from LabZY (nanoMCA-II). The distance from the X-ray tube to the center of the interrogation zone is estimated to be 20.5 cm and the distance from the detection to the center of the interrogation zone is estimated to be 18.5 cm. The angle between the X-ray tube and the detector is determined to 80°. These geometrical characteristics are given since they play an important role in the calibration procedure to be detailed further on.

The lasing experiments are carried out on Inconel 625 solid plates and powders from Oerlikon (MetcoAdd 625A reference). This powder is characterized by values of the D10, D50 and D90 volume percentiles of respectively 21 µm, 34.7 µm and 57.5 µm. The samples are placed in the centre of the chamber. Two lasing powers and two scan velocities have been considered, respectively: 150 W, 250 W and 0.025 m/s, 0.2 m/s. The higher lasing velocity is a more representative value of an industrial machine while the lower lasing velocity allow us to have a more important power density at the interaction surface, favoring the fumes generation. In the same line of thought, the choice of two laser powers was made to highlight significant variation within the ED-XRF signals. Finally, in addition to the Nitrogen (N) gas, Helium (He) is also considered due to its low density inducing less attenuation of the X-ray and therefore favouring the acquisition of ED-XRF signals. In addition, He is also known for reducing the number of spatters and the size of the vapour nanocondesates due to its higher thermal conductivity [7].

2.3. ED-XRF measurement method

The left hand side of Fig. 3 presents an example of an ED-XRF spectrum obtained from a 163 s long measurement on Inconel 625 powder with a laser power of 250 W and 0.025 m/s scanning velocity (blue curve). Fluorescence lines corresponding to the Chromium (Cr Kα at 5.41 keV), Iron (Fe Kα at 6.40 keV) and Nickel (Ni Kα at 7.48 keV) elements can be identified. A large part of the spectrum is due to scattering events associated with the surroundings and the use of polychromatic X-ray source (see red bar on energy axis). Shown superimposed in orange is the result of a similar ED-XRF acquisition but without any lasing. We call this type of acquisition “Background” (X-ray ON, laser OFF). Such a background is due to the presence in the surroundings of various sources of Cr, Fe and Ni that contribute also significantly to the counting (amplitude) of their respective fluorescence lines. Therefore, to be sensitive only to the useful laser related signal, a background measurement has to be acquired and subtracted.

For every ED-XRF measurement, a net counting N_n of the fluorescence lines of interest (here Cr and Ni lines) is calculated as follow. First, for a selected fluorescence line, for instance Ni Kα (7.48 keV), a Gaussian fitting is made in order to calculate the Full Width at Half Maximum (FWHM) and the amplitude of the peak, as described by the green dotted line in the right hand side of Fig. 3. Based on the norm ISO-11929 [8], a Region Of Interest (ROI) is defined as 2.5 times the value of the FWHM, given here at 0.162 keV. Therefore a global counting N_g is given (the blue area). Then, the contribution of the noise, N_b is estimated by using two enlarged ROI (see yellow areas) at the right and left of the peak. Finally the net counting calculation is given by $N_n = N_g - N_b$.

2.4. ED-XRF calibration method

In order to attribute a mass fraction to each net counting, a calibration method has been set up, based on a numerical model. Indeed, it is complicated to conceive of physical standards representative of a LPBF fume. Therefore, to avoid transfer coefficients and biases potentially induced by a matrix effect, the choice was to elaborate a numerical calibration model. Then, by using the reference particle transport Monte-Carlo simulation code PENELOPE [9], representative configurations for the X-ray spectrum, flux, geometry, detector and detector collimation have been modelled. For the two atmospheres chemistry (N and He) of the interaction chamber, a fixed number of ten mass fraction values of simulated Ni and Cr materials have been considered. The Ni and Cr materials are assumed homogeneously distributed in the simulated interaction chamber. This amounts to forty simulation configurations with 10^{12} primary photons emitted by the X-ray source, simulated for each case. All Monte–Carlo simulations were performed with PENELOPE 2006 implemented on a Linux cluster. The most demanding configurations with low metallic mass fraction (below 0.01% in atmosphere) required up to 40 h and 50 processors Intel(R) Xeon(R) CPU E5-2680 v2 @ 2.80 GHz. The simulation result gives a probability density which corresponds to the probability for one primary photon to interact and to be detected. This value has to be converted in count in order to be used as calibration for the experimental data. To do so, we take into account the exact X-ray tube parameters that we used during the experimental campaign (voltage, power, target material) and the detector response in terms of energy resolution and efficiency. Then, with the spectrum converted, the net counting (N_n) of Cr and Ni Kα lines are estimated and the calibration curves can be built. They are shown in Fig. 4 with a specific zoom on the low mass fraction values. In this range, a linear trend curve describes very well the fluorescence net counting variation as a function of the Ni and Cr mass fraction. It is thus possible using these curves to attribute a given mass fraction to a given net count number for both Cr and Ni materials present in the fumes for both N and He atmospheres.

It should be mentioned that our assumption of constant number of atoms in the interrogation zone is a priori not representative of the experimental configuration, where assuming the melt pool temperature

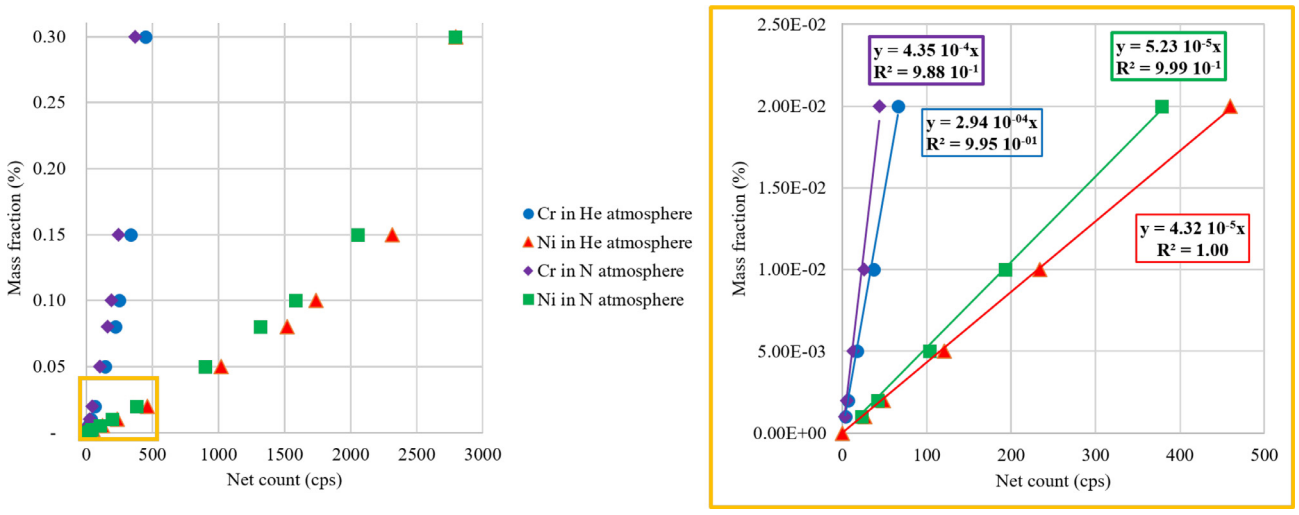

Fig. 4. Calibration curves for Ni Kα and Cr Kα lines in N and He atmosphere (left) with a zoom for low mass fraction (right) where linear variation occur.

Table 1
Net counting of Cr and Ni Kα line in count per second (cps) as function of laser power (P_{laser}) for Inconel 625 solid plate and powder in an N atmosphere with a lasing velocity of 0.025 m/s. Notice that at P_{laser} = 150 W on a solid plate the net counting of Cr Kα is not significant.

	Solid plate		Powder	
P_{laser} (W)	Cr Kα (cps)	Ni Kα (cps)	Cr Kα (cps)	Ni Kα (cps)
150	0.06 ± 0.23	2.33 ± 0.30	0.75 ± 0.14	2.40 ± 0.29
250	1.04 ± 0.25	5.20 ± 0.30	1.84 ± 0.39	9.20 ± 0.28

to be constant, the quantity of matter is expected to increase linearly with time. However, taking advantage of this linear behavior, calibration and experimental data can be compared assuming that the fumes concentration is evaluated at a time given by half the duration of the experiment.

3. Results and discussion

In a first approach, a low lasing velocity of 0.025 m/s was chosen, experiments being carried out on both a solid plate and a powder layer. As explained earlier the idea with the use of such an unconventionally low velocity is to maximise the power density delivered to the metallic sample to enhance Cr and Ni element evaporation and therefore their fluorescence detection. The measurement was produced in an N atmosphere with a lasing scanning square area of 20 × 20 mm^2 during 163 s. The Table 1 presents the net counting of the Cr and Ni Kα lines in count per second (cps). Repeatability measurements have been made for the tested lasing configuration. The net counting difference between two-repeatability measurements is taken into account in the error bar in addition to the statistical counting error. All uncertainty values appearing in the manuscript are given with an enlargement factor of 2.

For a laser power (P_{laser}) variation from 150 W to 250 W a significant increasing of the Cr and Ni Kα net counting is measured for the two types of Inconel 625 material (solid plate and powder), highlighting the impact of the laser power change. The Table 1 shows also the influence of the Inconel 625 material structure on the ED-XRF measurement. It appears that globally the fluorescence signal is significantly more important when the laser interacts with the powder compared to the Inconel 625 solid plate despite the fact that, on average the mass density of the powder should be of the order of 50% less compared to the plate. Such a result can tentatively be explained by a lower effective reflectivity of the powder compared to the solid plate, leading to a better absorption of the laser energy [10].

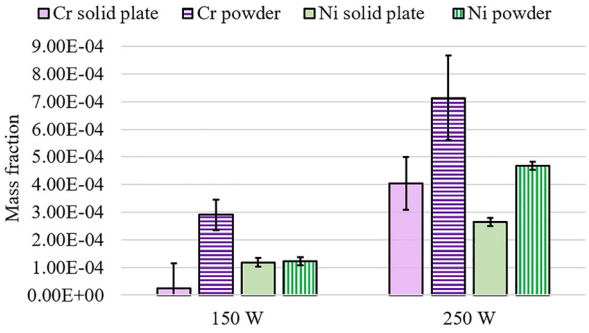

Fig. 5. Mass fraction of Cr and Ni elements present in the fumes during two LPBF process of Inconel 625 solid plate and powder at laser power of 150 W and 250 W with a lasing velocity of 0.025 m/s in an N atmosphere. Notice that the Cr mass fraction estimation of the solid plate case is not significant according to the net counting measurement from Table 1 (see red value). (For interpretation of the references to colour in this figure legend, the reader is referred to the web version of this article.)

To retrieve physical concentration values, the calibration curves (Fig. 4) are used. Figure 5 shows the variation of the Cr and Ni mass fractions detected in the fumes for the two laser powers at low lasing velocity on Inconel 625 solid plate and powder. When the laser power increases, the Cr and Ni proportions increase as well. Similarly, we estimate a higher proportion of Cr and Ni in the fumes when the laser interacts with powder.

In order to be more representative of an industrial LPBF setup, we consider now only Inconel powder and we increase the lasing velocity to 0.2 m/s for a lased area of 34 × 42 mm^2 during 78 s. Changing these parameters results in a diminution of the injected energy density. Therefore, in order to maximise the sensitivity of the ED-XRF measurement we decided to use He gas that allows a minimal attenuation of the fluorescence rays. For example, at the energy of the Cr Kα line of 5.41 keV, only 0.04% of the photons are attenuated by 5 cm of He gas, as compared to 14.03% for N atmosphere, 18.20% for dry air and 94.79% for Ar atmosphere. The Table 2 presents the net counting (cps) of the Cr and Ni Kα lines. The trends of these measurements are comparable to those of the low scanning configuration (see Table 1) with a correlation between the increase of the laser power and the Cr and Ni Kα net counting values. By applying the calibration on the net counting measurement, we obtain, as shown in Fig. 6, the variations of the Cr and Ni mass fractions detected in the fumes for the two laser powers at high lasing velocity on Inconel 625 powder.

Table 2
Net counting of Cr and Ni Kα line in count per second (cps) as function of laser power (P_{laser}) for Inconel 625 powder in an He atmosphere with a lasing velocity of 0.2 m/s.

P_{laser} (W)	Cr Kα (cps)	Ni Kα (cps)
150	0.88 ±0.15	4.55 ±1.20
250	1.14 ±0.32	7.68±1.41

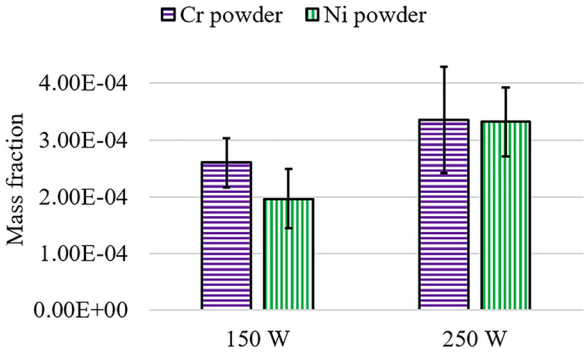

Fig. 6. Mass fraction of Cr and Ni elements present in the fumes during two LPBF process of Inconel 625 powder at laser power of 150 W and 250 W with a lasing velocity of 0.2 m/s in He atmosphere.

4. Comparison with an analytic physico-chemical model

To support the validity of the results of the mass fraction analysis presented before and therefore of our whole experimental approach and calibration method, we propose to confront them with a simple analytic physico-chemical model that can nevertheless capture some interesting features. The basic idea is to estimate the quantity of matter Q of the Cr and Ni elements that is present within the interrogation volume under the conditions presented before. To estimate the value of the interrogation volume, a Monte-Carlo method of 3D random sampling was used [11]. To start with, based on the work of Mayi et al. [12], we estimate the quantity of matter dQ/dt in mol/s that evaporates and condenses in form of fumes, written as:

$$\frac{dQ}{dt} = (1-\beta_R)\frac{P_{sat}}{\sqrt{2\pi M RT}} \times A_{spot} \tag{1}$$

where β_R represents the retro-diffusion coefficients, i.e. the fraction of the molecules that do not make it to the interrogation zone because they recondensate in the liquid pool, M is the molar mass (kg/mol), R the ideal gas constant (J/Kmol) and T the metallic bath temperature (K). As noted in Mayi et al. [12], depending on the local temperature and Mach numbers, the retro-diffusion coefficient is expected to vary from values close to $\beta_R = 1$ below the boiling point of the considered species down to $\beta_R = 0.18$ at high vapor pressures. Regarding the vapor pressure P_{sat} of pure elements, it can be calculated at a given temperature T according to the Clausius–Clapeyron relation:

$$P_{sat} = P_{atm} \exp\left[\frac{M\Delta_v H_m}{RT_v}\left(1-\frac{T_v}{T}\right)\right] \tag{2}$$

With P_{atm} the atmospheric pressure (Pa), $\Delta_v H_m$ the enthalpy of vaporization (J/mol) and T_v the boiling temperature under atmospheric pressure (K). Because our samples are alloys, Raoult's law has to be considered for the calculation of the Ni and Cr vapor pressure above the melt. Assuming that the fumes are solely generated from the laser spot area A_{spot} (even if it can be expected that the material located in the vicinity of the laser spot is also at high temperatures and thus prone to evaporation) it becomes possible to derive the mass concentrations of Ni and Cr within the fumes at a given temperature. The results are shown in Fig. 7 for both the He and N atmospheres and two β_R values ($\beta_R = 0.18$ and $\beta_R = 0.95$) using the boiling temperatures and enthalpies of vaporization of Ni and Cr from reference [13] listed in Table 3.

Table 3
The molar mass (M), the boiling points (T_v) and enthalpies of vaporization ($\Delta_{vap}H_m$) of Cr and Ni elements from [13].

	M (kg mol^{-1})	T_v(K)	$\Delta_v H_m$(J mol^{-1})
Cr	0.052	2755	347.10^3
Ni	0.059	3003	379.10^3

However, what is required to get an estimation of the melt pool temperature from the experimentally observed number of counts is an inverse model based on the calibration procedure. As mentioned above, we have to consider that, in the experimental conditions, the quantity of matter in the interrogation zone increases linearly with time, meaning that the time input for the model calculations should be taken as half the duration of the experiment.

From the also above mentioned assumption that the fumes are homogeneously distributed within the interaction chamber, the quantity of matter present within the interrogation volume derived from the model should be weighted by the ratio of the interrogation volume to the total chamber volume. From a mathematical standpoint, the interrogation volume is defined as the intersection between the X-ray cone-beam emission with the solid detector angle. Taking all these assumptions into account, the temperatures corresponding to the fumes mass concentration

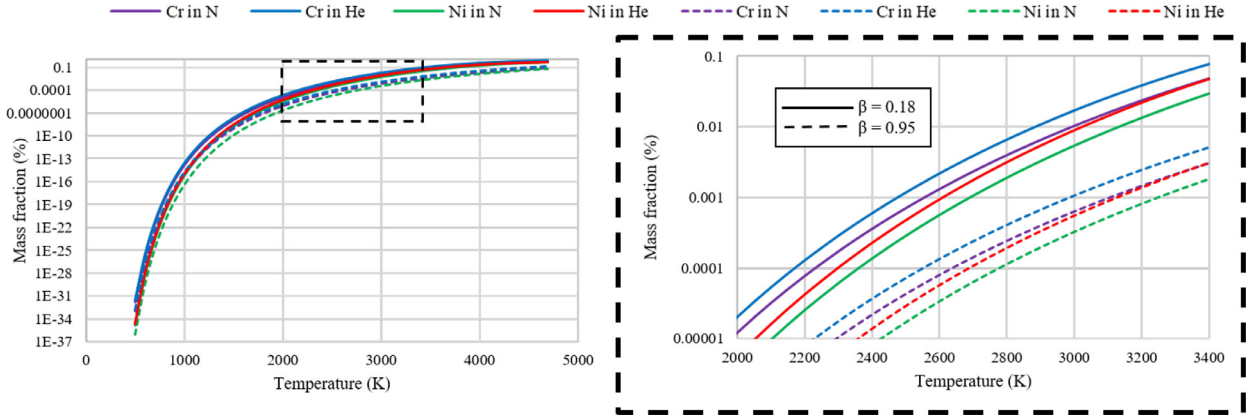

Fig. 7. Cr and Ni fumes mass fractions (%) as a function of the metallic bath temperature in both the He and N atmospheres. The dash lines correspond to $\beta = 0.95$ and the continuous lines correspond to $\beta = 0.18$.

Table 4
Metallic temperature bath estimation (K) in function of the mass fractions of Cr (wt_{Cr}) and Ni (wt_{Ni}) elements estimated by ED-XRF method with $\beta_R = 0.18$ and $\beta_R = 0.95$. Case of low laser velocity of 0.025 m/s in N atmosphere (see Fig. 5) on Inconel 625 solid plate and powder.

		Solid plate				Powder			
	P_{Laser}(W)	wt_{Cr}	T_{Cr}(K)	wt_{Ni}	T_{Ni}(K)	wt_{Cr}	T_{Cr}(K)	wt_{Ni}	T_{Ni}(K)
$\beta = 0.18$	150	NA	NA	$1.19\ 10^{-4}$	2380	$2.90\ 10^{-4}$	2370	$1.22\ 10^{-4}$	2390
	250	$4.05\ 10^{-4}$	2420	$2.65\ 10^{-4}$	2490	$7.14\ 10^{-4}$	2500	$4.68\ 10^{-4}$	2640
$\beta = 0.95$	150	NA	NA	$1.19\ 10^{-4}$	2810	$2.90\ 10^{-4}$	2835	$1.22\ 10^{-4}$	2975
	250	$4.05\ 10^{-4}$	2900	$2.65\ 10^{-4}$	2960	$7.14\ 10^{-4}$	3025	$4.68\ 10^{-4}$	3170

Table 5
Metallic temperature (K) bath estimation deduce from the mass fractions of Cr (wt_{Cr}) and Ni (wt_{Ni}) elements estimated by ED-XRF method with $\beta_R = 0.18$ and $\beta_R = 0.95$. Case of high laser velocity of 0.2 m/s in He atmosphere (see Fig. 6).

	P_{laser} (W)	wt_{Cr}	T_{Cr}(K)	wt_{Ni}	T_{Ni} (K)
$\beta = 0.18$	150	$2.60\ 10^{-4}$	2300	$1.97\ 10^{-4}$	2380
	250	$3.35\ 10^{-4}$	2320	$3.32\ 10^{-4}$	2450
$\beta = 0.95$	150	$2.60\ 10^{-4}$	2720	$1.97\ 10^{-4}$	2810
	250	$3.35\ 10^{-4}$	2760	$3.32\ 10^{-4}$	2900

from the calibration procedure presented earlier, are listed in Tables 4 and 5 using as done previously the two limiting retrodiffusion coefficient cases, namely $\beta_R = 0.18$ and $\beta_R = 0.95$.

Focusing first on the results for $\beta_R = 0.18$, it can be stated that the values listed in Tables 4 and 5, while of the expected order of magnitude, are a few hundredth of K below the boiling point of the respective elements, and thus not consistent with the hypothesis of large vapour pressure. On the other hand, the temperatures obtained assuming $\beta_R = 0.95$ are in the vicinity of the boiling temperatures of the respective elements (see Table 3) consistent with the fact that it is necessary to take a β_R value of the order of unity. An accurate determination of β_R is outside the scope of the present work, see [12] for a detailed discussion on the topic, but it is encouraging to see that the temperature values deduced from the simple physico-chemical model take reasonable values. Even more satisfying, temperatures deduced independently from Ni and Cr data remain within close bounds, with a difference around 100 K on average. In view of the numerous assumptions of the model, such a result was far from a priori obvious. In any case, taking into consideration the numerous assumptions involved the consistency between our experimental, calibration and model data is worth stating.

5. Conclusion and perspectives

The objective of this preliminary work was to propose a proof of concept of fumes monitoring during an LPBF process by ED-XRF. A significant net counting variation of the Kα fluorescence lines of Cr and Ni is established for variations of the laser power, scanning velocity and chamber atmosphere. To relate number of counts and fumes concentrations, a numerical calibration method has been developed. Finally, to gain some insights on the melt pool temperatures, a physico-chemical model is proposed, leading to consistent results between two independent measurements.

Regarding perspectives, our opinion is that the developed ED-XRF methodology could be extended to other metallic systems, such as Al-Zn where a significant differential evaporation can be expected. On the theoretical side, a further development would be to estimate, using again some type of mass balance, the composition of the solidified metal from the fumes measurements.

In addition to the LPBF process, our methodology could be adapted to the Electron Beam Powder Bed Fusion (EB-PBF), where the vacuum atmosphere should be favourable for the detection of material with low energy fluorescence lines. Away from LPBF, our approach could be fruitfully extended to WAAM or WLAM (Wire Laser Additive Manufacturing) configurations as well as welding processes.

Declaration of Competing Interest

The authors declare that they have no known competing financial interests or personal relationships that could have appeared to influence the work reported in this paper.

Data availability

Data will be made available on request.

Acknowledgments

This research was supported by the platform Additive Factory Hub (AFH) from Ile-de-France region, France.

References

[1] S. Ly, A.M. Rubenchik, S.A. Khairallah, G. Guss, M.J. Matthews, Metal vapor micro–jet controls material redistribution in laser powder bed fusion additive manufacturing, Sci. Rep. 7 (1) (2017) 1–12.
[2] S. Clijsters, T. Craeghs, S. Buls, K. Kempen, J.-P. Kruth, In situ quality control of the selective laser melting process using a high-speed, real-time melt pool monitoring system, Int. J. Adv. Manuf. Technol. 75 (5) (2014) 1089–1101.
[3] P. Lott, H. Schleifenbaum, W. Meiners, K. Wissenbach, C. Hinke, J. Bültmann, Design of an optical system for the in situ process monitoring of selective laser melting (SLM), Phys. Procedia 12 (2011) 683–690.
[4] C.L.A. Leung, S. Marussi, M. Towrie, J. del Val Garcia, R.C. Atwood, A.J. Bodey, J.R. Jones, P.J. Withers, P.D. Lee, Laser-matter interactions in additive manufacturing of stainless steel SS316l and 13–93 bioactive glass revealed by in situ X-ray imaging, Addit. Manuf. 24 (2018) 647–657.
[5] V.N. Lednev, P.A. Sdvizhenskii, R.D. Asyutin, R.S. Tretyakov, M.Y. Grishin, A.Y. Stavertiy, S.M. Pershin, In situ multi-elemental analysis by laser induced breakdown spectroscopy in additive manufacturing, Addit. Manuf. 25 (2019) 64–70.
[6] C. Vanhoof, J.R. Bacon, U.E.A. Fittschen, L. Vincze, 2020 atomic spectrometry update–a review of advances in X-ray fluorescence spectrometry and its special applications, J. Anal. At. Spectrom. 35 (9) (2020) 1704–1719.
[7] S. Traore, M. Schneider, I. Koutiri, F. Coste, R. Fabbro, C. Charpentier, P. Lefebvre, P. Peyre, Influence of gas atmosphere (Ar or He) on the laser powder bed fusion of a Ni-based alloy, J. Mater. Process. Technol. 288 (2021) 116851.
[8] R. p. Technical Committee ISO/TC 85, Nuclear energy. Subcommittee SC 2, Determination of the Characteristic Limits (decision Threshold, Detection Limit and Limits of the Confidence Interval) for Measurements of Ionizing Radiation–fundamentals and Application, ISO, 2010.
[9] F. Salvat, J.M. Fernández-Varea, J. Sempau, Penelope-2008: a code system for monte carlo simulation of electron and photon transport, in: Workshop Proceedings, Barcelona, Spain, vol. 30, 2008.
[10] J. Trapp, A.M. Rubenchik, G. Guss, M.J. Matthews, In situ absorptivity measurements of metallic powders during laser powder-bed fusion additive manufacturing, Appl. Mater. Today 9 (2017) 341–349.
[11] F.A. Balogun, A. Brunetti, R. Cesareo, Volume of intersection of two cones, Radiat. Phys. Chem. 59 (1) (2000) 23–30.
[12] Y.A. Mayi, M. Dal, P. Peyre, M. Bellet, C. Metton, C. Moriconi, R. Fabbro, Laser-induced plume investigated by finite element modelling and scaling of particle entrainment in laser powder bed fusion, J. Phys. D 53 (7) (2019) 075306.
[13] Y. Zhang, J.R.G. Evans, S. Yang, Corrected values for boiling points and enthalpies of vaporization of elements in handbooks, J. Chem. Eng. Data 56 (2) (2011) 328–337.